AMERICAN JOURNALS
Open Access, Peer Reviewed Journals

American Journal of Research in Humanities and Social Sciences
ISSN (E): 2832-8019 Volume 25, | June - 2024

PRIMARY HEPATIC NEUROENDOCRINE TUMORS: CONTRASTING PATHOLOGY WITH CT AND MRI CHARACTERISTICS

Turgunov B. Sh.
Baratova G. Q.
Mo'minova J. A.
Soqiyev S. A.

A B S T R A C T

Rarely, neuroendocrine cells, the pancreas, and the gastrointestinal system are the sites of origin for neuroendocrine carcinoma (NEC). Even though it looks like an adenocarcinoma, well-differentiated NEC exhibits more benign biological behavior [1]. Undifferentiated NECs, however, may have invasive and metastatic features, according to one report [2]. Compared to NEC, primary hepatic neuroendocrine tumors (PHNET) are less common, grow more slowly, and have the potential to progress into malignancy. Carcinoid syndrome affects a very small percentage of people. PHNETs and hepatocellular carcinoma (HCC) share similarities on CT and MRI scans; however, patients with PHNETs tend to have a better prognosis. Because CT and MRI scans are sensitive in identifying primary liver lesions and metastases, these methods may assist medical professionals in determining the best course of treatment and increase patient survival.

K E Y W O R D S

Introduction

Materials and procedures

Examine the populace

29 patients (13 men and 16 women; median age: 47.2 years) with PHNETs were hospitalized to Samarkand State Medical University Hospital between May 2004 and December 2013. Of these 29 patients, 5 cases had carcinoid syndrome, 7 patients reported pain in the right upper abdomen, 9 patients complained of stomach discomfort, 6 patients had routine ultrasounds that revealed PHNETs, and 2 patients had CT scans of their chests that revealed liver tumors. Every patient had a hepatectomy or a liver puncture guided by CT or ultrasonography. Immunohistochemistry and histology verified the existence of PHNETs. Alpha-feto protein (AFP) levels in the serum were normal (less than 40 ng/ml), the hepatitis B antigen virus was negative, and there was no sign of liver cirrhosis.

CT protocol for PHNETs

Abdominal helical CT examinations were performed with multi-detector row scanners (Light Speed Ultra, GE Healthcare, Milwaukee, Wis). Food and water were deprived 4–6 h before enhanced CT examinations. To show contrast between the liver and digestive tract, an oral positive

contrast agent (500 ml water combined with 10 ml iopromide, Bayer Healthcare) was used. The patients were in the supine position, scanning range was from the right diaphragm to the kidney, slice thickness was 5 mm with helical scan and the slice thickness of the reconstruction image was 1.25 mm with a pitch of 0.984:1. All patients received nonionic intravenous contrast aterial (Ultravist, 300mgI/ml, Bayer Technology & Engineering Company Limited, Berlin, Germany), which was administered at a rate of 4 mL/s (90–120 mL total dose) using a mechanical power injector (Medrad, Pittsburgh, PA, USA) set at 230 mAs and 120 kVp. Thereafter, hepatic arterial, portal venous phase, and delayed phase images were acquired with delays of 25 s, 50–60 s, and 2–3 min, respectively. The slice thickness and reconstruction slice thickness were the same with unenhanced CT.

MRI protocol for PHNETs

Diffusion-weighted MR imaging was performed before dynamic imaging, using a single-shot spin-echo echo planar imaging (EPI) sequence with b factors of 0 and 800 s/mm2 along the three orthogonal directions. The sequence was obtained within two breath-holding periods for the whole liver. The parameters included: TR =4000 ms, TE = 66 ms, matrix = 138 × 128, FOV = 32 to 38 cm adapted to individual body size, twenty-four slices for each b factor for entire liver, thickness = 6 mm, interslice gap = 0.6 mm, average = 2, bandwidth = 1735 Hz/pixel, and acquisition time = 24 s for each breath-holding period. The parallel imaging algorithms (GRAPPA) with an acceleration factor of 2 were added. Spectral fat saturation was employed systematically to suppress the chemical-shift artifacts. ADC maps regarding isotropic images were automatically acquired and all mean ADCs of the lesions were measured on those maps. For patients who did not hold their breath within 24 s, we induced slices for each b factor and added the thickness of the slice and the gap. The acquisition time in scanning the whole liver for hold-breath one time could be reduced to 16 s.

Results

Using pathology and the 2010 WHO classification of PHNET, eight cases were defined as G1, 10 cases were defined G2, and 11 cases were defined G3. All 19 singular lesions (G1 8 cases, G2 7 cases and G3 4 cases) underwent surgical resection. The maximum diameter of the mass was 8 cm with a clear border. Twelve lesions were predominantly solid, one case showed calcification, and the remaining 6 cases were cystic-solid or predominantly cystic. HE staining of G1 lesions revealed well-differentiated round or ovoid cells arranged in nests and glandular duct or chrysanthemum formation. The mitosis rate ranged from 0 to 2 per 10 high power fields. In G2 lesions, the cell arrangements were irregular, with mild differentiation and minimal nuclei atypia. The mean mitosis rate was 10 (range: 4 to 16) per 10 high power field. G3 lesions were poorly differentiated with large nuclei and the mean mitosis rate was 27 (range: 22 to 40) per 10 high power field.

Based on CT imaging (Table 1) and MRI data (Table 2), all G1 liver lesions were singular with only one lesion located in left lobe and remaining lesions the in right lobe. A CT scan of one patient revealed central necrosis in the absence of hemorrhage and cystic change. One patient
had calcification and mild enhancement. For the other 6 patients, pre- and post-enhanced CT densities were homogenous and showed marked enhancement while the dynamic-contrast enhancement curves of seven lesions (87.5 %) appeared as type III. All lesions showed enhanced capsules in the delayed phase of postenhancement CT while one lesion appeared plateau-like type. Seven out of eight patients with G1 PHNETs underwent a MRI examination in addition to a CT scan (Table 2). The lesions showed

hypointensity on preenhanced T1-weighted and homogeneous, mildly high intensity or high intensity on T2-weighted imaging. Enhancements
on post-enhanced MRI scans had markedly high (6 cases) and mildly high intensities (1 case). The ADC values in the liver tumors were lower than the surrounding normal liver tissue (1.39 ± 0.20 × 10−3 mm2/s versus (2.0 ± 0.38 × 10−3 mm2/s). All lesions showed enhanced
capsules in the delayed phase of post-enhancement MRI scans. These data further confirm that G1 lesions were benign or low-grade malignant tumors and distinguishable from hepato-cellular carcinoma.

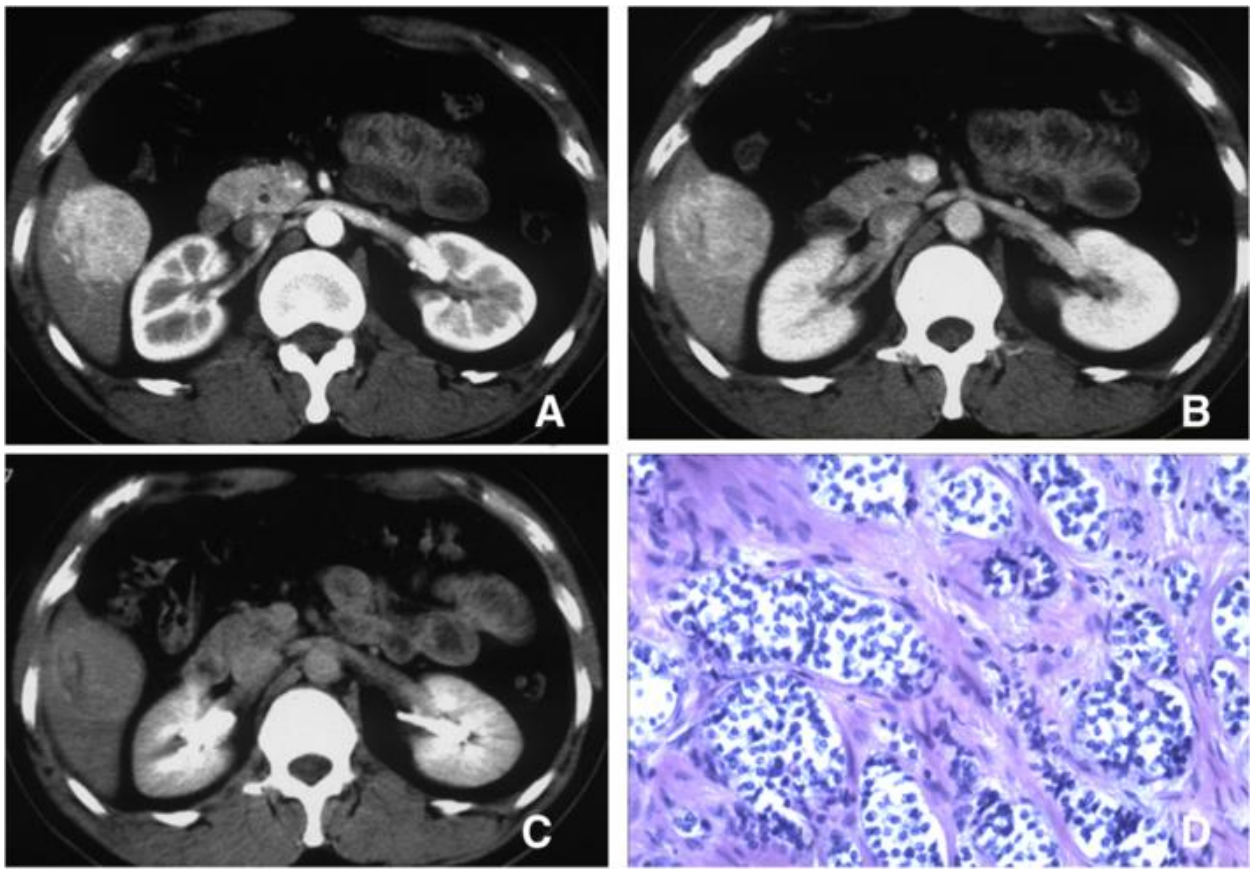

Fig. 1 CT scan and histology of grade 1 PHNET. Post-contrast CT image of the arterial phase (a), the portal venous phase (b) and the delayed phase (c) shows marked enhancement in the PHNET relative to the liver parenchyma (right lobe at the arterial phase), and slight hyperattenuation relative to the surrounding liver parenchyma in the delayed phases. The integrity of the capsule is maintained. The mitosis rate shows up as hypo-density and no enhancement on the dynamic enhanced CT scan. HE staining of the tumor (d) shows tumor cells arranged as solid nests, consistent cell size and mitosis rate was 1/10 HPF. Magnification: D = 100X

Four out of eleven cases with G3 PHNETs were singular and the remaining seven cases appeared as diffuse, multi-nodular or marginal-ring enhancement on CT. Three multi-nodular cases were misdiagnosed as metastases and two cases were misdiagnosed as hepatocellular carcinoma with diffuse intra-liver metastases. However, one case had tumor thrombus in the portal vein in and 10 cases had

necrosis, heterogeneous hypo-intensity on T1WI and high intensity or mildly high intensity on T2WI as illustrated by MRI. On T2WI, one case showed the liquid-liquid level and another showed hypo-intensity in the lower part. All patients (9/9) showed multi-nodular or
marginal-ring markedly high enhancements on postenhanced MRI and at the margins or solid area of the tumor dynamic-contrast enhancement curves (type III).

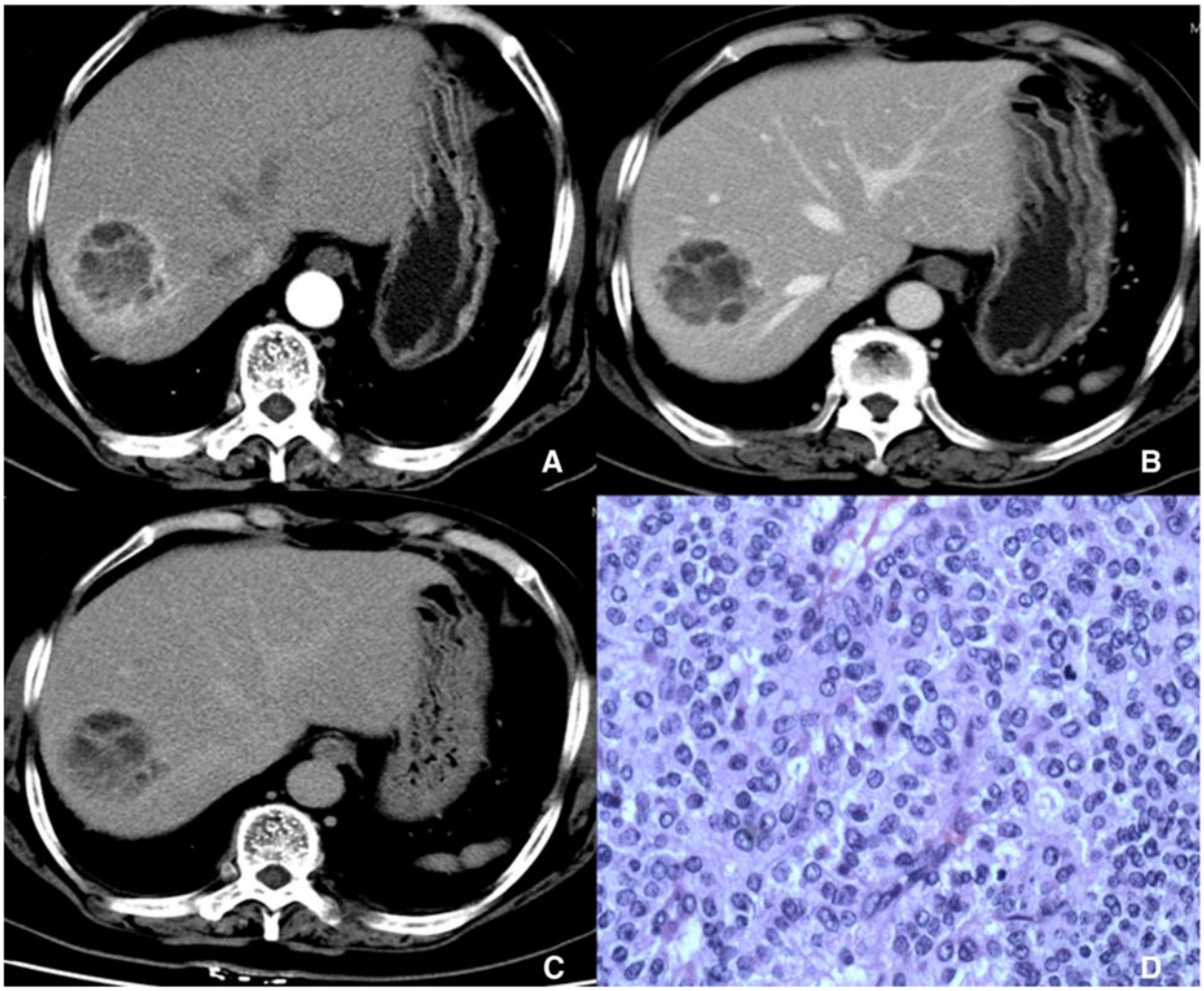

Fig. 2 CT scan and histology of grade PHNET. Post-contrast CT image of the arterial phase (a), portal venous phase (b), and delayed phase (c). The PHNET (5.4 × 5.7 cm in size) has marginal ring-like and septal enhancements (right lobe). Arterial phases reveal a wash-in pattern at the periphery of the tumor. Portal phase and delayed phase reveal slight peripheral hyper-attenuation compared with the surrounding liver parenchyma. HE staining shows liver tumor cells arranged in an island. Atypia and nucleoli were not readily apparent but nuclear chromatins were distributed in fine granules (d). Mitosis rate was 2–3/10 HPF and blood sinus was abundant in the intestinal with no hemorrhage

Discussion

In this work, we found that careful imaging with CT and MRI scans could accurately reflect the histological features of primary hepatic neuroendocrine tumors (PHNETs) and increase the likelihood of a correct diagnosis. A tumor that originates from neuroendocrine cells is a neuroendocrine tumor

(NET). There are two types of NETs: neural neuroendocrine tumors and epithelial neuroendocrine tumors. Hepatic NECs have a better prognosis than hepatocellular
carcinoma [9], but characteristic local invasion, metastases, and serious complications of carcinoid syndrome contribute to the poor outcome of patients with hepatocellular carcinoma [10–12]. Furthermore, positive staining for chromaffin granule (CgA), synaptophysin (Syn), and neuron specific enolase (NSE) are important in the pathological diagnosis of PHNET. Zhu Z et al. [13] reported that PHNETs appear as a single tumor. Our MRI and CT scans revealed that G1
PHNETs usually have single lesions in the right lobe whereas G3 PHNETs commonly have multiple diffuse lesions or one large tumor accompanied by several satellite lesions. PHNETs are difficult to distinguish from liver cancer [14]. Kim JE et al. [6] reported variation in the CT images of hepatic neuroendocrine tumors that did not correlate with their pathologic diagnoses. In these cases, PHNETs showed arterial enhancements that resembled hepatocellular carcinoma and delayed phase enhancements that resembled a cholangiocarcinoma. In our study, we had six cases of PHNETs (three cases were G2 and three cases were G3) that were misdiagnosed as
metastases.

References

1. Akhmedov YA, Ataeva SKh, Ametova AS, Bazarova SA, Isakov HKh THE HISTORY OF THE DEVELOPMENT OF RADIATION DIAGNOSTICS. Web of scientist: International scientific research journal. 2021;2:34-42.
2. Akhmedov YA, Rustamov UKh, Shodieva NE, Alieva UZ, Bobomurodov BM Modern Application of Computer Tomography in Urology. Central Asian journal of medical end natural sciences. 2021;2(4):121-125.
3. Ataeva SKh, Ravshanov ZKh, Ametova AS, Yakubov DZh Radiation visualization of chronic joint diseases. Central Asian journal of medical end natural sciences. 2021;2(2):12-17
4. Hamidov OA, Diagnostics of injuries of the soft tissue structures of the knee joint and their complications. European research. Moscow. 2020;1(37):33-36.
5. Khamidov OA, Khodzhanov IYu, Mamasoliev BM, Mansurov DSh, Davronov AA, Rakhimov AM The Role of Vascular Pathology in the Development and Progression of Deforming Osteoarthritis of the Joints of the Lower Extremities (Literature Review). Annals of the Romanian Society for Cell Biology, Romania. 2021;1(25):214 – 225
6. Khamidov OA, Akhmedov YA, Ataeva SKh, Ametova AS, Karshiev BO Role of Kidney Ultrasound in the Choice of Tactics for Treatment of Acute Renal Failure. Central Asian journal of medical end natural sciences. 2021;2(4):132-134
7. Khamidov OA, Akhmedov YA, Yakubov DZh, Shodieva NE, Tukhtaev TI DIAGNOSTIC POSSIBILITIES OF USES IN POLYKYSTOSIS OFKIDNEYS. Web of scientist: International scientific research journal. 2021;2(8):27-33
8. Khamidov OA, Ataeva SKh, Ametova AS, Yakubov DZh, Khaydarov SS A Case of Ultrasound Diagnosis of Necrotizing Papillitis. Central Asian journal of medical end natural sciences. 2021;2(4):103-107
9. Khamidov OA, Ataeva SKh, Yakubov DZh, Ametova AS, Saytkulova ShR ULTRASOUND EXAMINATION IN THE DIAGNOSIS OF FETAL MACROSOMIA. Web of scientist: International scientific research journal. 2021;2(8):49-54

10. Khamidov OA, Mirzakulov MM, Ametova AS, Alieva UZ Multispiral computed tomography for prostate diseases. Central Asian journal of medical end natural sciences. 2021;2(2):9-11
11. Khamidov OA, Normamatov AF, Yakubov DZh, Bazarova SA Respiratory computed tomography. Central Asian journal of medical end natural sciences. 2021;2(2):1-8
12. Khamidov OA, Urozov UB, Shodieva NE, Akhmedov YA Ultrasound diagnosis of urolithiasis. Central Asian journal of medical end natural sciences. 2021;2(2):18-24
13. Khamidov OA, Yakubov DZh, Alieva UZ, Bazarova SA, Mamaruziev ShR Possibilities of Sonography in Differential Diagnostics of Hematuria. Central Asian journal of medical end natural sciences. 2021;2(4):126-131
14. Khamidov OA, Yakubov DZh, Ametova AS, Bazarova SA, Mamatova ShT Application of the Ultrasound Research Method in Otorhinolaryngology and Diseases of the Head and Neck Organs. International Journal of Development and Public Policy. 2021;1(3):33-37
15. Khamidov OA, Yakubov DZh, Ametova AS, Turdumatov ZhA, Mamatov RM Magnetic Resonance Tomography in Diagnostics and Differential Diagnostics of Focal Liver Lesions. Central Asian journal of medical end natural sciences. 2021;2(4):115-120
16. Rustamov UKh, Shodieva NE, Ametova AS, Alieva UZ, Rabbimova MU US-DIAGNOSTICS FOR INFERTILITY. Web of scientist: International scientific research journal. 2021;2(8):55-61
17. Rustamov UKh, Urinboev ShB, Ametova AS Ultrasound diagnostics of ectopic pregnancy. Central Asian journal of medical end natural sciences. 2021;2(2):25-28
18. Abdurakhmanovich, K. O., & ugli, G. S. O. (2022). Ultrasonic Diagnosis Methods for Choledocholithiasis. Central Asian Journal Of Medical And Natural Sciences, 3(2), 43-47.
19. Abdurakhmanovich, K. O., & ugli, G. S. O. (2022). Ultrasound Diagnosis of the Norm and Diseases of the Cervix. Central Asian Journal Of Medical And Natural Sciences, 3(2), 58-63.
20. Yakubov Doniyor Javlanovich, Juraev Kamoliddin Danabaevich, Gaybullaev Sherzod Obid ugli, and Samiev Azamat Ulmas ugli. 2022. “INFLUENCE OF GONARTHROSIS ON THE COURSE AND EFFECTIVENESS OF TREATMENT OF VARICOSE VEINS”. Yosh Tadqiqotchi Jurnali 1 (4):347-57.
21. Yakubov , J., Karimov , B., Gaybullaev , O., and Mirzakulov , M. 2022. Ultrasonic and radiological picture in the combination of chronic venous insufficiency and osteoarthritis of the knee joints. Academic Research in Educational Sciences. 5(3), pp.945–956.
22. Yakubov D. Z., Gaybullaev S. O. The diagnostic importance of radiation diagnostic methods in determining the degree of expression of gonarthrosis //UZBEK JOURNAL OF CASE REPORTS. – С. 36.
23. Якубов Д. Ж., Гайбуллаев Ш. О. Влияние посттравматической хондропатии на функциональное состояние коленных суставов у спортсменов. Uzbek journal of case reports. 2022; 2 (1): 36-40. – 2022.
24. Alimdjanovich, R.J., Obid , K., Javlanovich, Y.D. and ugli, G.S.O. 2022. Advantages of Ultrasound Diagnosis of Pulmonary Pathology in COVID-19 Compared to Computed Tomography. Central Asian Journal of Medical and Natural Science. 3, 5 (Oct. 2022), 531-546.
25. Kadirov J. F. et al. NEUROLOGICAL COMPLICATIONS OF AIDS //Journal of new century innovations. – 2022. – Т. 10. – №. 5. – С. 174-180.